atmosphere

MDPI

Article

Field Measurement of the Near-Ground Wind Characteristics Around Landing Center During Typhoon 'Mangkhut' (1822)

Xu Lei [1,2,*], Ming Nie [3], Xiaoyu Luo [3], Wenping Xie [3], Lian Shen [1,2,*], Yinfeng Xie [1,2] and Qiyi Yang [4]

[1] Hunan Provincial Key Laboratory for Big Data Smart Application of Natural Disaster Risks Survey of Highway Engineering, Changsha University, Changsha 410022, China
[2] School of Civil Engineering, Changsha University, Changsha 410022, China
[3] Electric Power Science Research Institute of Guangdong Power Grid, Guangzhou 510080, China
[4] School of Civil Engineering, Changsha University of Science and Technology, Changsha 410114, China
* Correspondence: leixuemail@163.com (X.L.); z20171185@ccsu.edu.cn (L.S.); Tel.: +86-133-1875-0873 (X.L.); +86-136-5735-8399 (L.S.)

Abstract

A two-dimensional ultrasonic anemometer was installed at a height of 20 m on a wind measurement tower in Haiyan Town, Jiangmen, to monitor flow conditions in typhoon Mangkhut (1822) before and after landfall. Mean wind speed, wind direction, turbulence intensity, gust factor, turbulence integral scale, and turbulence power spectral density were derived and analyzed before and after landing. The results show that the central wind speed time history before and after landfall exhibits significant differences, and the mean wind direction undergoes a reverse change of about 180°. The mean downwind and crosswind turbulence intensity before landing were 0.25 and 0.22, respectively, and 0.20 and 0.16 after landing. The associated mean downwind and crosswind gust factors were 1.70 and 0.61 before landing, and 1.55 and 0.46 after. These differences before and after landing are considered significant, and both turbulence intensity and gust factor showed a certain decreasing trend with the increase in wind speed. The relationship between turbulence intensity and gust factor, though somewhat scattered, was basically consistent with the commonly used Ishizaki and Choi empirical formulas. Mean streamwise and crosswind turbulence integral scales before landfall were 218 m and 100 m, respectively, and 198 m and 177 m after. They showed a weak increasing trend with increase in mean wind speed. Power spectra before and after landing were basically consistent. Comparisons with standard forms were inconclusive, though the von Karman spectrum appeared to be slightly superior to the others, particularly as the wind speed and turbulence integral scale increased.

Keywords: typhoon 'Mangkhut'; field measurement; near ground wind field; mean flow; turbulence characteristics

Academic Editor: Alan Robins

Received: 20 November 2025
Revised: 9 January 2026
Accepted: 10 January 2026
Published: 14 January 2026

1. Introduction

Typhoons, as a natural disaster with a devastating impact on infrastructure, cause immense direct and indirect economic losses annually. In recent years, influenced by climate change, there has been an increasing trend in their frequency and intensity [1]. The genesis and development of typhoons are influenced by complex factors such as sea surface temperature, water vapor evaporation, air current rotation, and topography, exhibiting significant individual variability that makes accurate analysis through theory and numerical simulation challenging [1]. The most direct and effective technical means

to prevent typhoon disasters currently is to obtain a certain number of typhoon wind field characteristic parameter samples through field measurements, derive corresponding statistical laws, and thereby guide structural wind-resistant design specifically.

For structural wind-resistant design, due to civil building height limitations, typhoon measurements primarily focus on near-ground wind field characteristics. As early as 2000, Pang et al. [2] conducted an analysis of the mean and turbulent wind characteristics at a 20 m high observation point in Shanghai, Pudong, at the path center of typhoons "Prapiroon" and "Jelawat", concluding that near-ground turbulence intensity and gust factors are high, with turbulence integral scales around 80 m, and the horizontal (downwind and crosswind) turbulence power spectral density functions are largely consistent with the Simiu spectrum. Subsequently, Shi et al. [3], Li and Hu et al. [4–6] conducted measurements of the wind field characteristics at the landing centers of three typhoons around 2006 (Damrey, Chanchu, Prapiroon), typhoon "Kalmaegi" in 2008, and "Hagupit" through wind speed observation points set at heights ranging from 5 m to 30 m near the ground. The main conclusions were that wind field characteristics differ significantly before and after landfall, with typhoon turbulence, gust factors, and turbulent spectral density significantly exceeding the corresponding values specified in wind loading codes, and the measured wind speed spectra matching well with the Von Karman spectrum; analyses of different parameters of turbulent wind speed and spatial correlation were conducted, providing quantitative correction suggestions for near-ground typhoon wind fields based on the measurement results.

Xiao and Li et al. [7,8] conducted measurements of the mean and turbulent wind field characteristics of typhoon "Hagupit" in 2008 over the near-sea surface, comparing and analyzing the differences in wind field characteristics before and after the eyewall and the peripheral wind field. Additionally, within the framework of the Monin–Obukhov similarity theory, they proposed a data-driven method for modeling the turbulent wind speed spectrum of the typhoon boundary layer by considering design benchmark conditions, validating the method through parameterization of the theoretical formula with measurements from typhoon "Hagupit". Xu et al. [9] also validated the rationality of this method based on the near-ground measured turbulent wind speed spectrum of typhoon "Bailu". Wang et al. [10–12] conducted measurements of the near-ground turbulent wind field at heights ranging from 10 m to 40 m at the landing center areas of typhoons "Muifa", "Meari", and "Haikui", analyzing the relationships between turbulence intensity, gust factor, turbulence integral scale, peak factor, mean wind speed, and height above ground, discussing in detail the characteristics of the measured power spectral density function segments and the applicability of empirical spectra. In recent years, measurement studies have continued, with Li et al. [13], He et al. [14], Sun et al. [15], and Shao et al. [16] conducting near-ground (10–40 m height range) wind field measurements at the landing centers of typhoons "Soulik", "Haima", "Fitow", "Matmo", and "Mekkhala", focusing on the turbulent wind characteristics before and after landfall, concluding that downwind turbulence intensity and gust factor decrease with increasing wind speed, stabilizing after the mean wind speed exceeds 10 m/s, with turbulence integral scales showing no clear relationship with mean wind speed and turbulence, and the measured typhoon power spectra generally matching well with the Von Karman empirical spectrum. Chen et al. [17] and Li et al. [18] discussed the influence of ground roughness on typhoon wind field characteristics based on measurement data from typhoons "Haitang", "Nesat", and "Soulik" landing near mountainous areas.

Huang et al. [19] used the landing center and peripheral wind field observation points of typhoon "Rammasun" (1409) to conduct statistical analysis on the mean wind speed, wind direction, wind speed profile, turbulence intensity, gust factor, and other turbulent

wind field characteristics of the typhoon. Zhang et al. [20] conducted a detailed analysis of the near-sea near-ground wind field during the progression of typhoon "Soudelor" based on an array of anemometers at the Xiamen Dadeng Island typhoon observation point, systematically studying the relationships between various parameters and the distance from the typhoon center as well as observation height. Cai and Huang et al. [21] established a quantitative mapping relationship between the statistical parameters of stationary and non-stationary wind speed models and verified the accuracy of the theoretical relationship based on the wind speed data measured by the Shenzhen meteorological gradient tower during typhoon "Sura" from 31 August to 2 September 2023. This study provides a quantifiable parameter conversion framework for modeling non-stationary wind fields in typhoons.

Regarding the typhoon "Mangkhut" (1822) discussed in this paper, the existing relevant measured research results are as follows: Zeng et al. [22] used the best path dataset of tropical cyclones from the Japan Meteorological Agency, precipitation data from stations provided by the China Meteorological Administration, and circulation and sea surface temperature data from the European Meteorological Center, analyzing their path, intensity changes, sea surface temperature background, circulation characteristics, water vapor transport characteristics, and dynamic thermal physics field. Zhao et al. [23] and He et al. [24] conducted experimental research on the global structure and wind field characteristics affecting tropical cyclones in southern China based on long-term observation data from sounding balloons, radar wind profiler, and other equipment. Taking typical typhoons ("York" and "Mangkhut") as examples, the horizontal and vertical main structural characteristics of the system were examined, revealing the double eyewall structure, eyewall displacement phenomenon, and axial asymmetric changes in the structure after landfall. Xie and Duan et al. [25,26] analyzed the vertical distribution pattern of wind field characteristics during the invasion process of super typhoon "Mangkhut" (1822) based on the measured wind speed time history data from the 356 m high Shenzhen Meteorological Gradient Tower (SZGMT). In addition, they also used discrete wavelet transform (DWT) and ensemble empirical mode decomposition (EEMD) methods to extract time-varying mean wind speed from wind speed sequences, analyzed the mean wind speed profile, turbulence intensity, gust factor, turbulence integral scale, turbulent wind speed spectrum, and other fluctuation characteristics, and compared the results with the stationary model method (SMM). Wang and Cui et al. [27,28] took a long-span bridge structure in the Pearl River Estuary of Guangdong Province as the background and analyzed the wind characteristic parameters of the typhoon, such as the mean wind speed, wind direction angle, turbulence intensity, gust factor, and peak factor, based on the 32 h wind speed time history data collected by the wind environment monitoring system in real time during the landing process of typhoon "Mangkhut" (1822). However, it is worth noting that the above-mentioned studies on typhoon "Mangkhut" (1822) are not characteristics of its eye center wind field. It is worth noting that some scholars such as Fang et al. [29], Liang et al. [30], and Li et al. [31] have analyzed the changes in the near-surface boundary layer and atmospheric stability during typhoons to explore their impact on the mean and turbulent wind fields near the ground. The study showed that the changes in the underlying surface near the landing point significantly affected the character of the internal boundary layer (IBL), including parameters closely related to the determination of structural wind loads, such as wind speed, turbulence intensity, and turbulent wind speed spectrum. In addition, the evolution of atmospheric stability during a typhoon may also influence the characteristics of the wind field.

In summary, long-term typhoon measurement studies have enriched the parameter sample database; however, existing data are still very limited, especially for near-ground,

near-center wind fields during typhoon landings. It is that deficiency that is addressed in this paper. We present and analyze high-frequency data from an ultrasonic anemometer data installed as a height of 20 m on a transmission tower near the landing center of typhoon "Mangkhut" (1822). Features discussed include wind speed, wind direction, turbulence intensity, gust factor, turbulence integral scale, and power spectral density function before and after the typhoon landing. The aim is to provide accurate and effective references for typhoon simulation and experimental research, as well as typhoon-resistant design of coastal infrastructure. Structure of the paper: The measurements are discussed in Section 2, with Section 3 dealing with data analysis, while Sections 4–6, respectively, study the measured mean wind speed and direction at the center of the typhoon, as well as the time-domain characteristics of the fluctuating wind field (turbulence intensity, gust factor, and turbulence integral scale) and frequency-domain characteristics (turbulence power spectrum).

2. Introduction and Measurement Overview of Typhoon "Mangkhut"

Typhoon "Mangkhut" was the 22nd typhoon of 2018. It formed in the mid-Pacific Ocean and moved in a northwest direction, creating landfall along the Taishan coast around 17:00 on September 16 (as a severe typhoon, with maximum wind speed of 45 m/s). Its path is shown in Figure 1a. The measurements were made at a height of 20 m above ground level, at about 10 km inland from the landing point. At this distance inland, the internal boundary layer (IBL) is likely to be more than 20 m deep. The tower and anemometer are shown in Figure 1b. Details of the tower location and surrounding terrain are shown in Figure 1c.

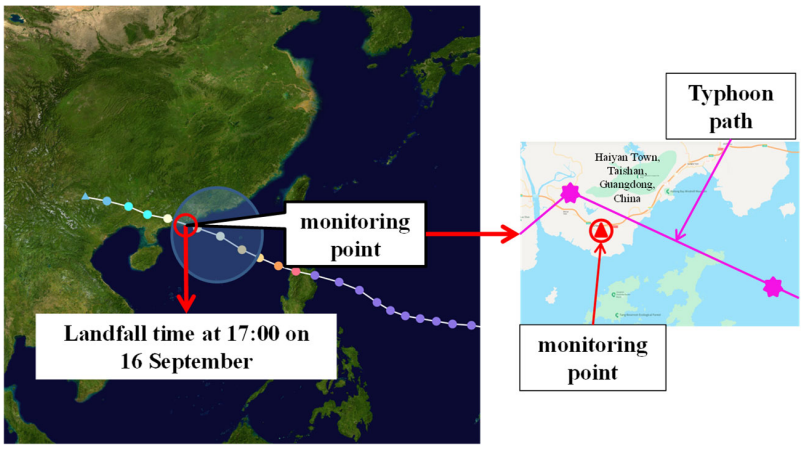

(**a**)

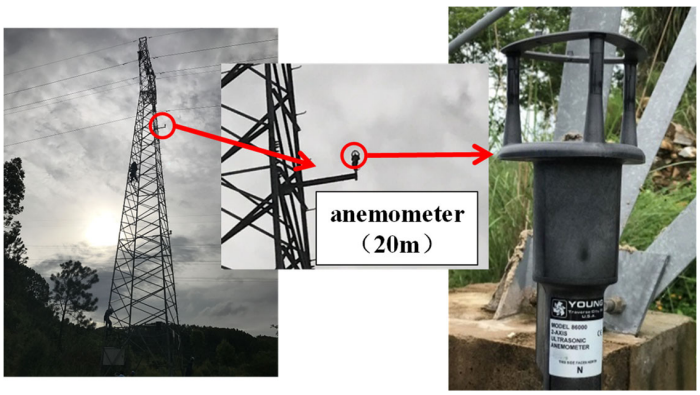

(**b**)

Figure 1. *Cont.*

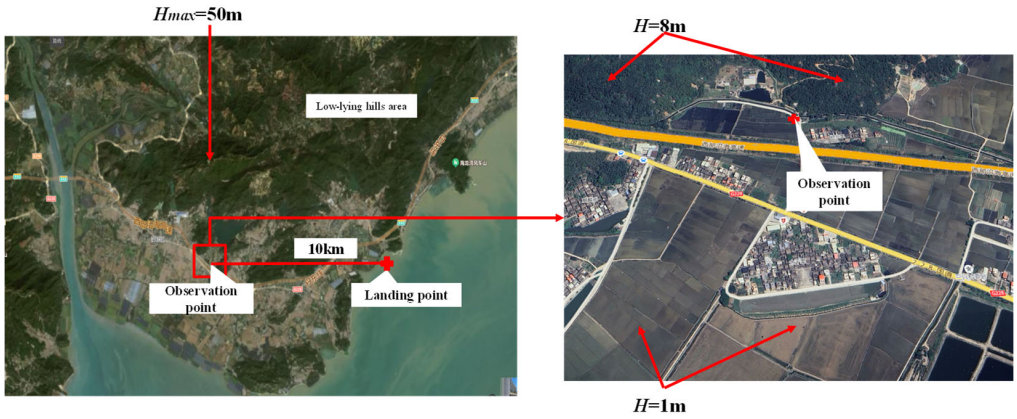

(**c**)

Figure 1. (**a**). The path followed by Typhoon 'Mangkhut'; (**b**) the measurement tower and anemometer; (**c**) the surrounding terrain.

Based on the National Meteorological Center of China's prediction of the typhoon's path and empirical judgment, the typhoon wind field characteristic observation system was preemptively selected and deployed at a height of 20 m on a wind measurement tower located in a flat area in Haiyan Town, Taishan City, the predicted landing center. The site was chosen for its open surroundings which is free from obstructions, to facilitate an on-site measurement study of the typhoon's center landing process. The system successfully captured the time history of horizontal wind field changes at the eye of the typhoon from 10:45 on the 16 September to 10:45 on the 17 September, encompassing the period before and after the typhoon's landfall. The ultrasonic anemometer, a YOUNG MODEL 86,000 two-dimensional ultrasonic anemometer with a sampling frequency of 120 Hz and a path length within the range of 85~100 mm, was installed facing true north; this means a zero-degree wind direction angle corresponds to true north, with the wind direction angle increasing clockwise. The field measurement system is depicted in Figure 1, and the original collected data of horizontal wind speed and direction are shown in Figure 2.

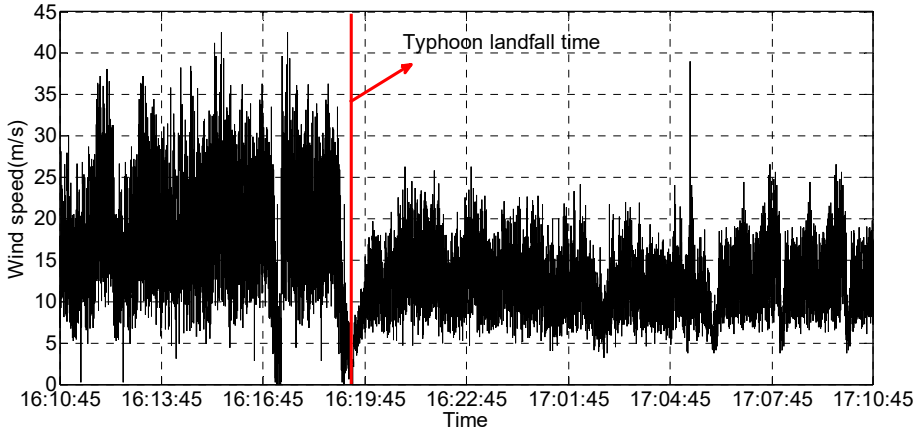

(**a**)

Figure 2. *Cont.*

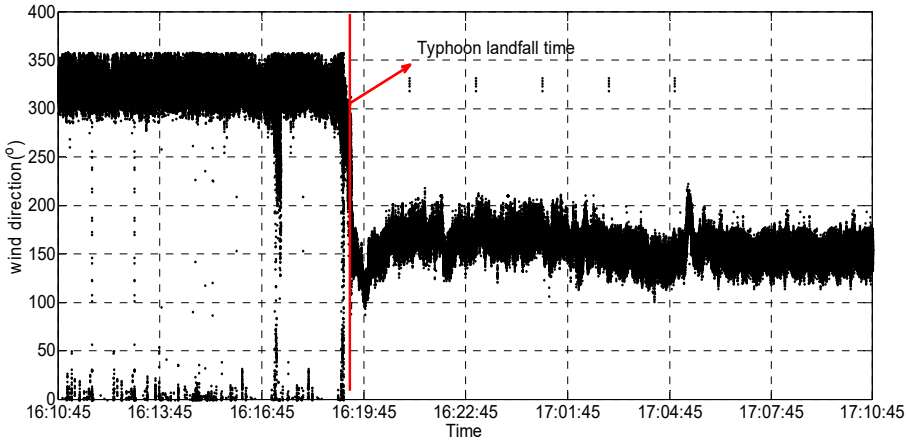

(**b**)

Figure 2. Original data on wind speed and direction at 20 m height measurement point. (**a**) Raw wind speed data; (**b**) raw wind direction data.

3. Method for Processing Measured Data

Unlike traditional wind cups or propeller anemometers, ultrasonic sensors do not have rotating components, making them theoretically less susceptible to the effects of precipitation (such as raindrops, hail), adhesion, or freezing. However, raindrops may scatter or absorb ultrasonic energy. Note that this can lead to errors in recorded speed and direction. This interference is more significant in heavy rainfall or dense raindrop environments, which may cause instantaneous data fluctuations. For this issue, the author has carried out pre-processing on the abnormal data, and the processing flow of this method for abnormal data is as follows:

Firstly, using the method of data segmentation, the measured data is divided into several 3 s data segments.

Then, take the mean and mean square value for each 3 s data segment.

Finally, compare the absolute value of each measured data point after subtracting the mean value with the three-fold mean square value. If it is less than the three-fold mean square value, the data point is considered normal, and if it is greater than the three-fold mean square value, it is considered abnormal. The result of the data point is corrected to mean plus mean square value.

For the measured data samples, the vector mean method is employed to analyze the mean wind speed and direction. Assuming the anemometer records the horizontal wind speed samples as instantaneous wind speed $u(t)$ and wind direction angle $\alpha(t)$, the wind speed can be orthogonally decomposed into components in the x and y directions as follows:

$$u_x(t) = u(t)\cos\alpha(t) \tag{1}$$

$$u_y(t) = u(t)\sin\alpha(t) \tag{2}$$

Taking 10 min as the fundamental time interval, and assuming the horizontal mean wind speed and wind direction angle are U and α, respectively, they can be calculated from the component results of the aforementioned equations as follows:

$$U = \sqrt{u_x^2(t) + u_y^2(t)} \tag{3}$$

$$\cos\alpha = \frac{u_x(t)}{U} \tag{4}$$

The corresponding downwind turbulent wind speed $u_t(t)$ and crosswind turbulent wind speed $v_t(t)$ can be expressed, respectively, as follows:

$$u_t(t) = u_x(t)\cos\alpha + u_y(t)\sin\alpha - U \tag{5}$$

$$v_t(t) = -u_x(t)\sin\alpha + u_y(t)\cos\alpha \tag{6}$$

The description of turbulence field characteristics mainly includes several characteristic parameters. The first one is turbulence intensity I that measures the relative intensity of wind speed fluctuations (random fluctuations) relative to the mean wind speed; it is a dimensionless parameter used to characterize the strength of atmospheric turbulence. The second one is gust factor G, which is a statistical parameter that describes the intensity of wind speed fluctuations, specifically representing the ratio or relative fluctuation in gusts (short-term maximum wind speed) to steady winds (mean wind speed). The third one is turbulence integral scale L, which is the core parameters that characterize the spatial or temporal scale of dominant eddies in turbulent flow fields, mainly reflecting the mean scale of dominant eddies and characterizing the distribution of turbulent energy. The corresponding downwind and crosswind turbulence intensities $I_i(u,v)$, as well as the gust factors $G_u(t_g)$ and $G_v(t_g)$, can be expressed, respectively, as follows:

$$I_i = \frac{\sigma_i}{U}(i = u, v) \tag{7}$$

$$G_u(t_g) = 1 + \frac{\max(u(t_g))}{U} \tag{8}$$

$$G_v(t_g) = \frac{\max(v(t_g))}{U} \tag{9}$$

In the equation, $i = u,v$ represents downwind and crosswind directions, respectively. σ_i represents the root mean square of the turbulent wind speeds $u(t)$ and $v(t)$; G_u, G_v represent downwind and crosswind gust factors, respectively; t_g is the gust duration used in the calculation, typically taken as t_g = 3 s.

Additionally, this paper also analyzes the measure of the mean size of eddies in the near-surface airflow—the turbulence integral scale—which is expressed as follows:

$$L_i = \frac{U}{\sigma_i^2}\int_0^{\mu} R(\tau)d\tau(i = u, v) \tag{10}$$

In the equation, $L_i(u,v)$ represents the downwind and crosswind turbulence integral scale, respectively; μ is the upper limit of the integral, taken as the point where the correlation coefficient drops to 0.05; $R(\tau)$ is the autocorrelation function of the wind speed time history.

4. Characteristics of the Mean Wind Field at the Center of Typhoon

4.1. Mean Wind Speed

The time history curves of the 10 min mean wind speed and direction before and after the typhoon's landfall are shown in Figure 3. The red solid line indicates the position at the time of the typhoon eye center landfall. At the moment of landfall, the mean wind speed rapidly decayed to its lowest value, and after landfall, the wind speed significantly weakened compared to before landfall, indicating that the measurement point was within the central landfall area of this typhoon. The 10 min mean wind speed in the strong wind area of the eyewall was mainly concentrated between 18 m/s and 23 m/s.

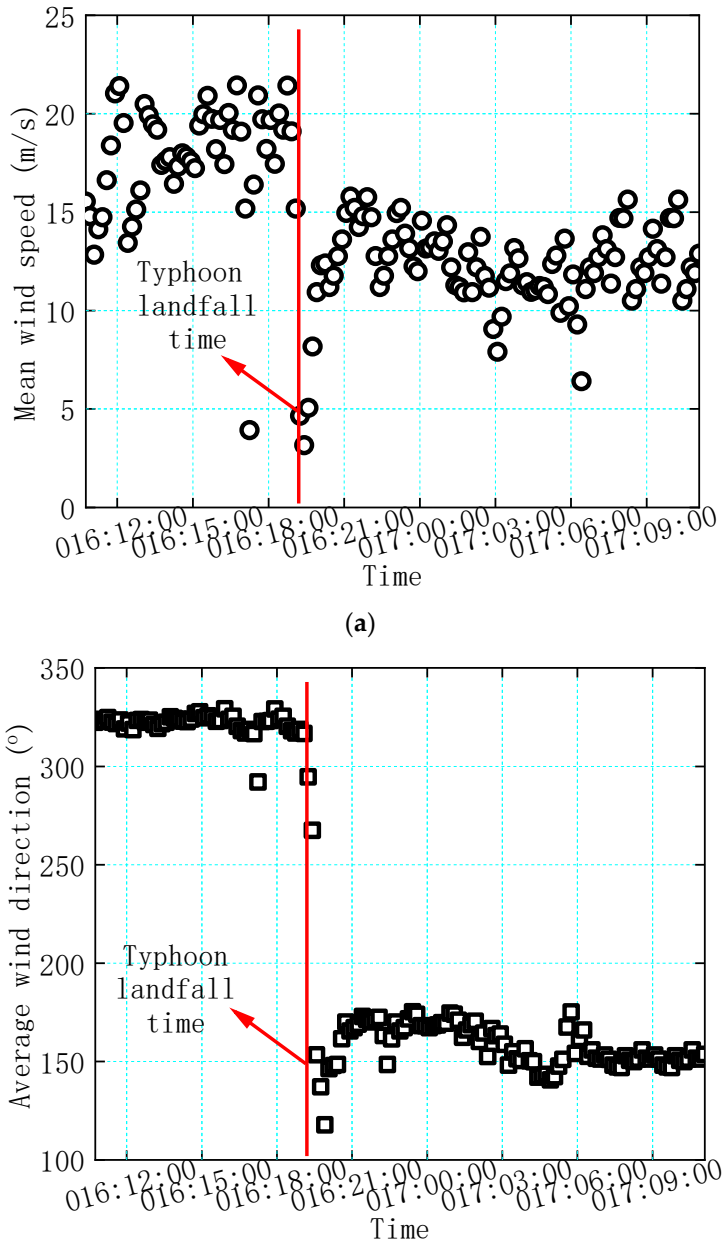

Figure 3. Mean wind speed and direction time history curve of measuring point before and after typhoon 'Mangkhut' landfall; these are 10 min mean values at a location 10 km inland of the point of landfall; (**a**) mean wind speed (20 m); (**b**) mean wind direction (20 m).

4.2. Mean Wind Direction

At the time of the typhoon's landfall, the wind direction at the measurement point reversed. Before landfall, the wind direction was mainly concentrated between 300° and 350°, while after landfall, it was mainly between 130° and 160°. The change in wind direction before and after landfall was approximately 180°, primarily due to the opposite direction of airflow on either side of the eyewall.

5. Time-Domain Characteristics of Turbulence at the Center of Typhoon

The time-domain characteristics of the turbulent wind field analyzed in this paper mainly include the turbulence intensity of downwind and crosswind turbulent wind

speeds, gust factors, and turbulence integral scales, which are of interest in structural wind engineering, as well as their interrelationships.

5.1. Turbulence Intensity

Figure 4a presents the time history curves of downwind and crosswind turbulence intensities at the 20 m height measurement point before and after the typhoon's landfall. Before landfall, the downwind and crosswind turbulence intensities were distributed between [0.20, 0.80] and [0.16, 0.44], with mean values of 0.25 and 0.22, respectively. After landfall, these values were distributed between [0.15, 0.30] and [0.12, 0.24], with mean values of 0.20 and 0.16, respectively. The crosswind turbulence intensity was significantly lower than the downwind, and the difference before and after landfall was pronounced. Figure 4b,c shows the variation in downwind and crosswind turbulence intensities with mean wind speed, including the best-fit linear relationships. From the figure, it can be seen that the downwind turbulence intensity showed a clear decreasing trend with increasing wind speed before and after landfall, while the crosswind turbulence intensity decreased significantly with increasing wind speed after landfall, but the trend was relatively weaker before landfall.

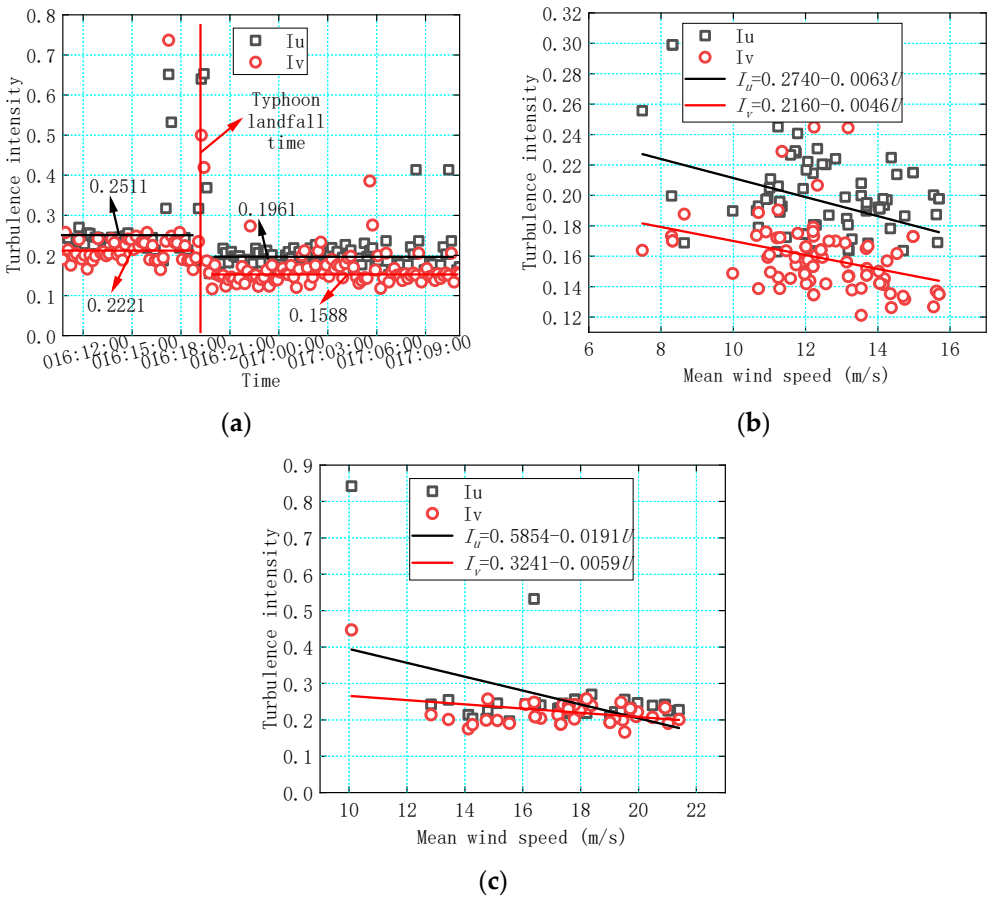

Figure 4. Time history of downwind and crosswind turbulence intensity and its variation with wind speed. (**a**) Variation in turbulence intensity over time; (**b**) relationship between turbulence intensity and wind speed before landfall; (**c**) relationship between turbulence intensity and wind speed after landfall.

In addition, the underlying surface may change from sea level to land before and after the typhoon makes landfall, which may also lead to the inner boundary layer effect (IBL) [29,30]. In addition, the replacement of cold and hot air currents during the typhoon's path from the ocean to land may also lead to the evolution of atmospheric stability [31],

which may affect turbulence intensity to a certain extent. It is worth noting that from the topographic map near the observation point (Figure 1), it can be seen that there is a low hilly area in the north with a poster height of about 8–50 m, while the south is mainly plain with a mean elevation of about 1 m. Before the typhoon made landfall, the wind direction changed from north to south, but after landfall, the wind direction changed. Therefore, it can be reasonably guessed that compared to the disturbance of hilly terrain in the upwind direction before landing, the corresponding turbulence intensity may decrease when the upwind direction is plain terrain after landing.

This paper includes the measured turbulence intensity results from eight typhoons with similar measurement point heights, distances from the typhoon center, surrounding topography, and mean wind speeds in Table 1, and also lists the corresponding results given by the standards in Table 2, comparing the measured downwind and crosswind turbulence intensity ratios with those above. Through the comparison in the tables, it is known that the measured values in this paper are basically close to the mean values of downwind and crosswind turbulence intensities and their ratios of the other eight typhoons in the table, with deviations of 0.0%, 5.1%, and 2.32% before landfall, and 20.3%, 23.4%, and 1.08% after landfall, respectively. Considering the specificity of different typhoons and testing and analysis errors, the measured results in this paper are basically consistent with previous measurements and have good representativeness. Through the comparison in Table 2, it is known that the Chinese standards for turbulence levels are smaller than those of the United States and Japan, and when the observation point in this paper is valued according to the suburban flat terrain (Class B), it is closer to the results of the US and Japanese standards. It is worth noting that the change in wind direction before and after the passing of the typhoon's eye may cause a change in the interference effect of the trees and low hills in the surrounding terrain and tower body. If the trees, low hills, and tower body are upstream of the incoming flow, they will have an interference effect on the anemometer, which will affect the turbulence intensity. If they are downstream, there will be no such effect. Therefore, after comprehensive analysis, it is considered that the measured results in this paper basically match the turbulence intensity values specified in the standards for Class B and C terrains, and they have good representativeness.

Table 1. Comparison of turbulence intensity measured in different typhoons.

Typhoon Name	Measurement Location, Topography	Mean Wind Speed (m/s)	Observation Height (m)	I_u, I_v	I_u:I_v
Jelawat (0008) [2]	Near typhoon center, Shanghai Pudong, flat suburban topography	6.0~11.6	20	0.29, 0.23	1:0.79
Prapiroon (0012) [2]	Shanghai Pudong, flat suburban topography	6.0~11.4	20	0.33, 0.30	1:0.91
Meari (1105) [10]	250 km from center, flat open topography	6.0~14.0	20	0.175, 0.155	1:0.89
Muifa (1109) [11]	Near typhoon center, flat open topography	5.0~23.0	20	/	1:0.65
Haikui (1211) [12]	Shanghai Pudong, flat suburban topography	8.0~15.0	20	0.24, 0.20	1:0.83
Soulik (1307) [13]	68 km from center, flat open topography	5.0~25.9	27	0.24, 0.19	1:0.79

Table 1. *Cont.*

Typhoon Name	Measurement Location, Topography	Mean Wind Speed (m/s)	Observation Height (m)	I_u, I_v	I_u:I_v
Soudelor (1513) [20]	100–400 km from center, flat open topography	6.0~8.0	20	0.30, 0.25	1:0.83
Mekkhala (2006) [16]	32.2 km from center, flat open topography	5.0~40.0	30	0.18, 0.14	1:0.78
Pre-landfall (This Study) Post-landfall (This Study)	30 km from center, flat open topography	8.0~15.0	20	0.25, 0.22 0.20, 0.16	1:0.79 1:0.80

Table 2. Comparison of turbulence intensity between different standards and field measurements (Z = 20 m).

	GB50009-2012 (China) $I_z = I_{10}\ (Z/10)^{-\alpha}$ [32]	ASCE/SEI 7-10 (USA) $I_{uz}=c\ (10/\bar{Z})^{1/6}$ [33]	AIJ-RLB-2004 (Japan) $I_{rZ} = 0.1\ (Z/Z_G)^{-\alpha-0.05}$ [34]	Measurement (This Study)
Class A terrain	0.110	0.134	0.146	0.25 (Before landfall) 0.22 (After landfall)
Class B terrain	0.126	0.178	0.177	
Class C terrain	0.188	0.267	0.218	
Class D terrain	0.229	0.401	0.289/0.403	

5.2. Gust Factor

Figure 5a presents the time history curves of the downwind and crosswind gust factors at the 20 m height measurement point before and after the typhoon's landfall. Before landfall, the downwind and crosswind gust factors were distributed within the ranges of [1.51, 2.62] and [0.42, 1.00], with mean values of 1.70 and 0.61, respectively. After landfall, these values were distributed within [1.35, 2.05] and [0.28, 0.88], with mean values of 1.55 and 0.46, respectively, showing some differences before and after landfall. Figure 5b,c illustrates the variation in the downwind and crosswind gust factors with mean wind speed and their trend fitting results. From the figure, it can be observed that both the downwind and crosswind gust factors exhibit a clear decreasing trend as the wind speed increases. It is worth noting that, similar to turbulence intensity, the gust factor also shows a decreasing trend before and after typhoon landfall.

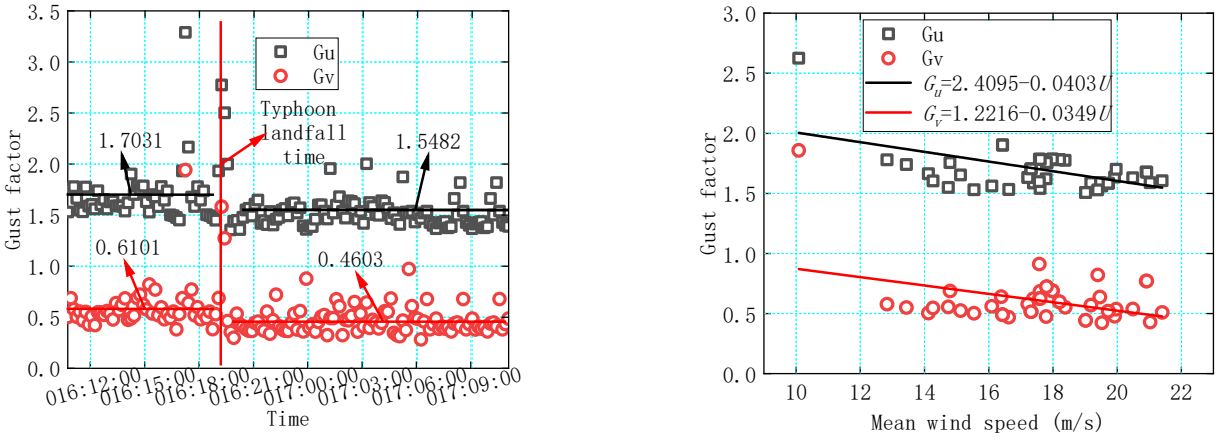

(**a**) (**b**)

Figure 5. *Cont.*

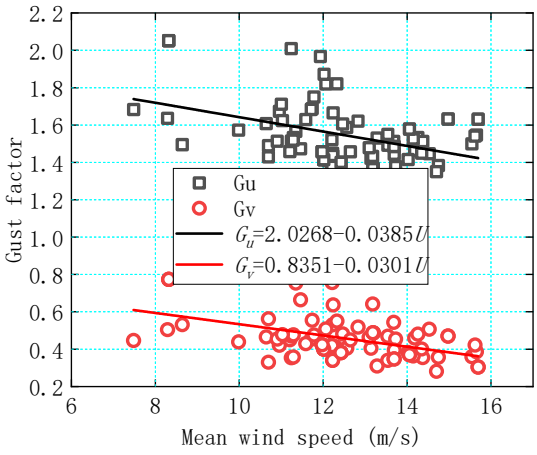

(**c**)

Figure 5. Time history of downwind and crosswind gust factors and their variation with wind speed. (**a**) Variation in gust factor over time; (**b**) relationship between gust factor and wind speed before landfall; (**c**) relationship between gust factor and wind speed after landfall.

5.3. Turbulence Integral Scale

Figure 6a presents the time history curves of the downwind and crosswind turbulence integral scales at the 20 m height measurement point before and after the typhoon's landfall. Before landfall, the mean values of the downwind and crosswind turbulence integral scales were 218 m and 100 m, respectively. After landfall, the mean values were 198 m and 177 m, respectively. It is noteworthy that the crosswind turbulence integral scale is generally significantly smaller than the downwind integral scale. Additionally, the downwind turbulence integral scale showed little change before and after landfall, while the crosswind turbulence integral scale exhibited considerable differences. Figure 6b,c illustrates the variation in the downwind and crosswind integral scales with mean wind speed. From the figure, it can be observed that before landfall, the downwind and crosswind turbulence integral scales showed a slight increasing trend with wind speed, whereas after landfall, they exhibited no pattern. However, overall, there is no significant correlation between the two.

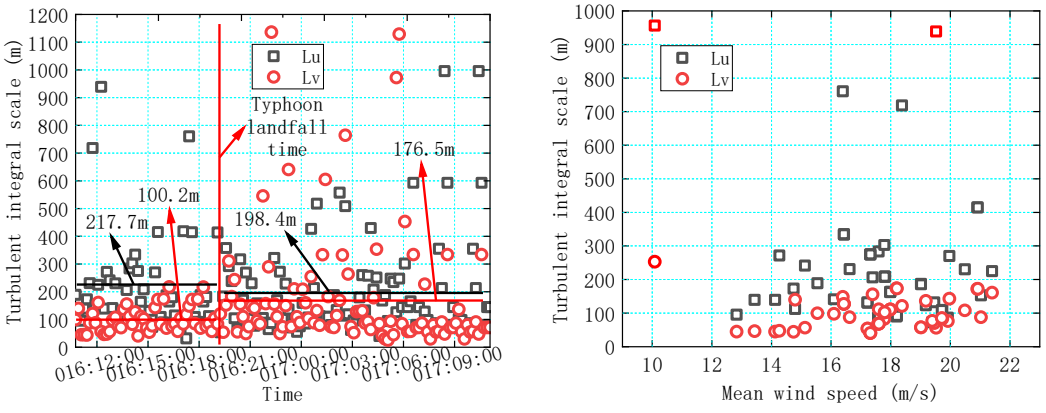

(**a**) (**b**)

Figure 6. *Cont.*

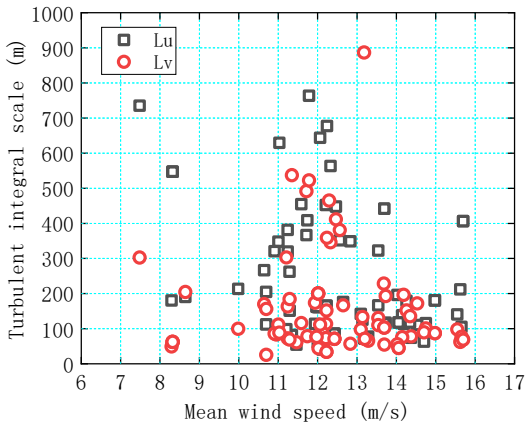

(**c**)

Figure 6. Time history of integral scale of downwind and crosswind turbulence and its variation with wind speed. (**a**) Variation in turbulence integral scale over time; (**b**) variation in integral scale with wind speed before landfall; (**c**) variation in integral scale with wind speed after landfall.

5.4. Relationship Between Turbulence Intensity and Gust Factor, Integral Scale

Ishizaki [35] and Choi [36] investigated the relationship between the gust factor G_u, turbulence intensity I_u, and gust duration t, and proposed empirical formulas, which are expressed as follows:

$$G_u = 1 + aI_u^b \ln(T/t) \tag{11}$$

In the formula, T is the mean wind time interval; t is the gust duration interval; a and b are undetermined parameters. Ishizaki suggested values of 0.5 and 1.0 for a and b, respectively, while Choi recommended a = 0.62 and b = 1.27.

This study used Equation (11) to fit the relationship between the measured turbulence intensity and gust factor before and after landfall. The fitting results are shown in Figure 7a,b. Before landfall, the fitting parameters for Equation (11) were (a, b) = (0.35, 0.70) and (0.51, 0.99). After landfall, the fitting parameters were (a, b) = (1.19, 1.51) and (0.56, 1.01). Comparing the fitting results with the empirical parameters, it is evident that Choi's suggested values are significantly lower, while Ishizaki's recommended values align better with the measured results. However, there is a notable deviation between the measured fitting parameters and the empirical values for the relationship between downwind turbulence intensity and gust factor.

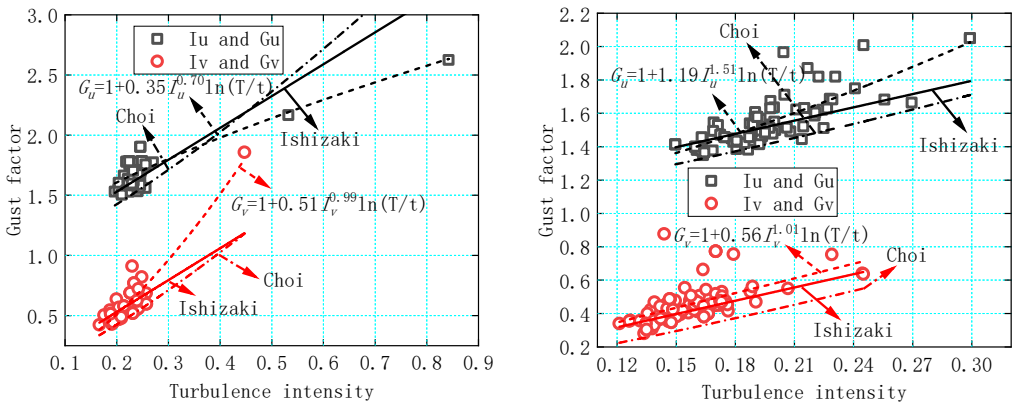

(**a**) (**b**)

Figure 7. The relationship between turbulence intensity and gust factor. (**a**) The relationship between gust factor and turbulence intensity before landfall; (**b**) the relationship between gust factor and turbulence intensity after landfall.

In Figure 8a,b, for the integral scale of turbulence before and after landing, it shows a certain degree of increasing trend with the increase in turbulence intensity, but the discreteness of turbulence integral scale also increases significantly with the increase in turbulence intensity. In addition, the measured turbulence intensity and the sample size of the integral scale in this article are not sufficient to fully demonstrate their interrelationships. At present, some existing on-site measurements of typhoons such as Pan et al. [2], Li et al. [13], and Xiao et al. [37] also indicate that there is no significant correlation between turbulence integral scale and turbulence intensity. Turbulence integral scale is the characteristic scale of the energetic eddies and defined as the integral of the two-point velocity correlation function from zero to the first zero crossing point. It describes the scale range of turbulent energy-containing eddies, which is closely related to the geometric boundaries, initial conditions, historical evolution, and other factors of the flow. The influencing factors are complex, resulting in high discreteness and randomness. In addition, there is insufficient data at large intensities to support meaningful conclusions.

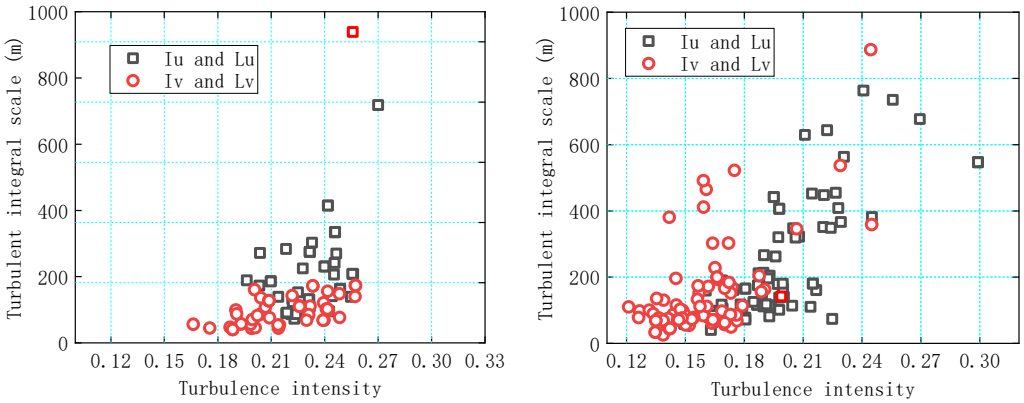

Figure 8. The relationship between turbulence intensity and turbulence integral scale. (**a**) The relationship between the integral scale of turbulence and turbulence intensity before landfall; (**b**) the relationship between the integral scale of turbulence and turbulence intensity after landfall.

6. Frequency-Domain Characteristics of Turbulence at the Center of Typhoon "Mangkhut"

The power spectral density function (PSD) of a turbulent wind field describes the energy distribution of wind speed fluctuation signals in the frequency domain, and is particularly important for analyzing the wind-induced vibration response of building structures. The frequency-domain characteristics of the turbulent wind at the center of typhoon "Mangkhut" can be represented by the power spectral density function, which is utilized to depict the proportional distribution of turbulent kinetic energy across various scale levels. Derived from Kolmogorov's theory [8], different forms of power spectra have been proposed, with the general formula presented as the following:

$$\frac{nS(n)}{\sigma^2} = \frac{Af}{[1 + Bf^{\alpha}]^{\beta}} \tag{12}$$

In the formula, $S(n)$ represents the power spectrum of the turbulent wind speed; σ is the root mean square of the corresponding turbulent wind speed; n is the frequency of the turbulent wind speed; f is the similarity law coordinate; A, B, α, β are fitting parameters.

Based on the aforementioned theory, various empirical parameter wind speed spectrum models such as Von Karman, Davenport, Kaimal, Simiu, and Panofsky have been obtained through actual measurement fitting [14,20].

The Japanese AIJ-2004 [34] adopts the Von Karman empirical spectrum, where the power spectral density of the downwind and crosswind turbulent wind speeds can be expressed as follows:

$$\begin{aligned} \frac{nS_u(n)}{\sigma_u^2} &= \frac{4f}{[1+70.8f^2]^{5/6}}; \\ \frac{nS_v(n)}{\sigma_v^2} &= \frac{4f(1+755.2f^2)}{(1+283.2f^2)^{11/6}} \end{aligned} \tag{13}$$

In the formula, $S_u(n)$ and $S_v(n)$ represent the power spectra of the downwind and crosswind turbulent wind speeds, respectively; σ_u, σ_v are the root mean squares of the downwind and crosswind turbulent wind speeds; $f = nL/U_z$, U_z is the 10 min mean wind speed at height z; for the downwind and crosswind turbulent wind speed spectrum calculation, L represents, respectively, the downwind turbulence integral scale L_u and crosswind turbulence integral scale L_v.

The Chinese GB50009-2012 [32] adopts the Davenport spectrum for the downwind turbulent wind speed spectra, which is expressed as follows:

$$\frac{nS_u(n)}{\sigma_u^2} = \frac{2f^2}{3(1+f^2)^{4/3}} \tag{14}$$

In the formula, $f = nL_u/U_z$, the recommended value for L_u in this empirical formula, is 1200 m. The meanings of the remaining symbols are consistent with those in Formula (13). It is worth noting that there is no empirical formula for the crosswind spectrum.

The American ASCE series adopts the Kaimal spectrum [30], which is expressed as follows:

$$\frac{nS_u(n)}{\sigma_u^2} = \frac{17.5f}{[1+33f]^{5/3}}; \frac{nS_v(n)}{\sigma_v^2} = \frac{4.16f}{(1+9.5f)^{5/3}} \tag{15}$$

In the formula, f is the Monin coordinates, where $f = nz/U_z$, and the meanings of the remaining symbols are consistent with those in Formulas (13) and (14).

The turbulence energy spectrum at large Reynold numbers can be divided into three regions: the energy-containing, the inertial, and the energy dissipation regions. Energy is fed from the mean flow to the largest scales through interaction between the mean shear and the large-scale eddies, which contain the majority of the turbulent kinetic energy. This energy is dissipated by viscosity at small scales in the dissipation region. Energy is passed from large to dissipation scales through a cascade process in the inertial range. In the results presented below, the inertial range commences at a frequency of about 0.1 Hz. In the inertial range the power spectrum, S(f), varies as f-5/3, or as f-2/3, when plotted as fS(f), as shown in the figures below. The ultrasonic anemometer has insufficient resolution to provide dissipation range data and any apparent fall-off from inertial range behavior is probably the result of that limitation.

From Figures 9–12, some regular observational results can be observed about the measured spectral characteristics before and after landfall:

Firstly, the turbulent wind speed spectrum characteristics before and after typhoon landfall are basically consistent, but compared to before the typhoon landfall, the measured spectrum and empirical spectrum after the typhoon landfall match better.

Secondly, the extent of the low-frequency energy-containing region (a1) and the inertial subrange (a2) are generally consistent under different mean wind speeds and turbulence integral scales. Both the downwind and crosswind wind speed spectra in the inertial subrange satisfy the Kolmogorov $-2/3$ law well.

Thirdly, for the downwind wind speed spectrum, the Von Karman and Kaimal empirical spectra show better agreement with the measured values than the Davenport spectrum, particularly in the low-frequency energy-containing region. This agreement becomes more

pronounced with increasing wind speed and integral scale. The reason lies in the fact that the Von Karman and Kaimal empirical spectra take into account the distribution of wind speed along the height and the integral scale factors, making their estimation of the typhoon's turbulent wind speed spectrum relatively more accurate and reasonable. For the crosswind wind speed spectrum, compared to Kaimal spectrum, the Von Karman empirical spectrum aligns better with the measured values. The crosswind Kaimal empirical spectrum shows significant deviations from the measured values and the Von Karman empirical spectra. Therefore, based on the above analysis, it can be concluded that the measured downwind and crosswind wind speed spectra before and after landfall align better with the Von Karman empirical spectrum.

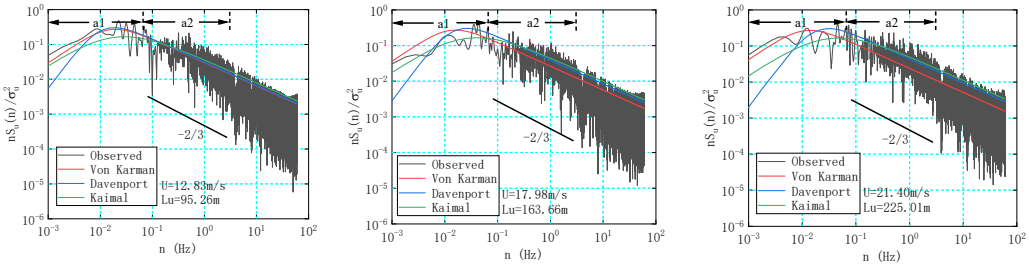

Figure 9. Downwind turbulent wind speed power spectral density function before the typhoon landfall.

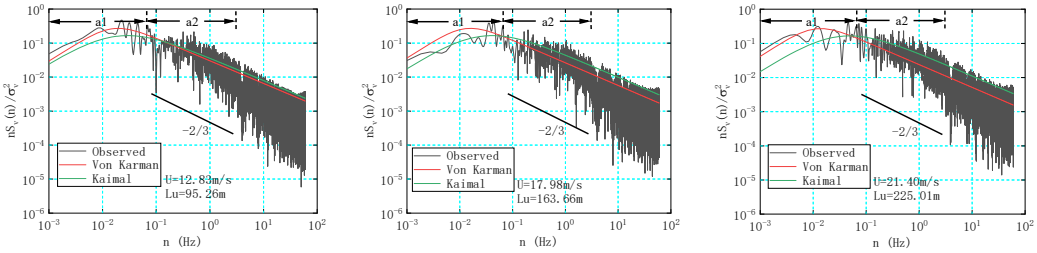

Figure 10. Crosswind turbulent wind speed power spectral density function before the typhoon landfall.

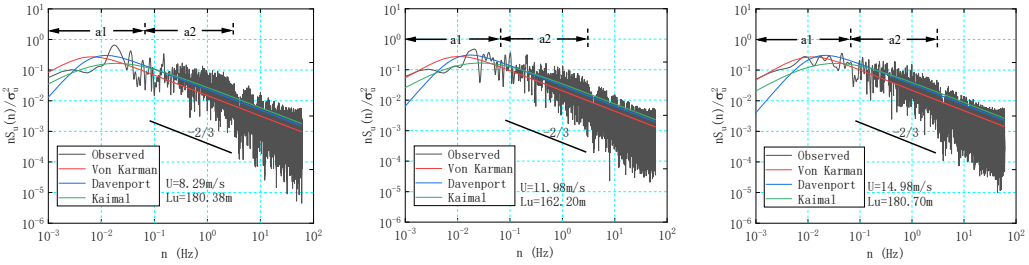

Figure 11. Downwind turbulent wind speed power spectral density function after the typhoon landfall.

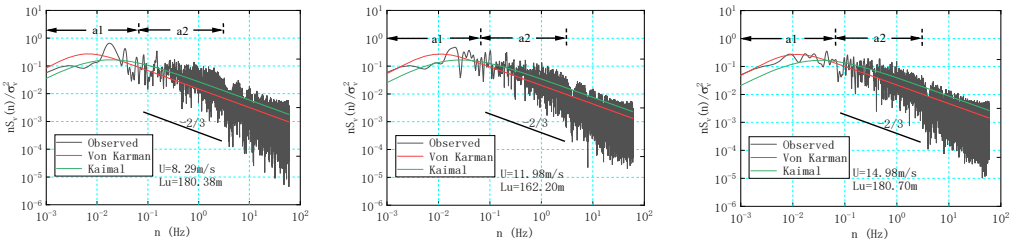

Figure 12. Crosswind turbulent wind speed power spectral density function after the typhoon landfall.

7. Conclusions

This research addressed the characteristic parameters of the near-surface wind field of typhoon 'Mangkhut' (1822) before and after landfall, including mean wind speed, wind direction and turbulence intensity, gust factor, turbulence integral scale, and turbulent wind

speed power spectral density, using a two-dimensional ultrasonic anemometer installed on an observation tower located 20 m above the ground in an open terrain area near the landing center. The main conclusions are as follows:

1. The time history of the central wind speed of the typhoon before and after landfall shows significant differences, with the mean wind direction angle reversing by approximately 180°.
2. The turbulence intensity and gust factor at the 20 m height measurement point show significant differences before and after landfall. Before landfall, the mean downwind and crosswind turbulence intensities were 0.25 and 0.22, respectively, while after landfall, they were 0.20 and 0.16. The mean gust factors before landfall were 1.70 and 0.61, respectively, and after landfall, they were 1.55 and 0.46. Both turbulence intensity and gust factor exhibit a decreasing trend with increasing wind speed. The measured turbulence intensity in this typhoon is generally consistent with previous measurements [2,10–13,16,20]. After excluding wind speed observation interference at the measurement point, it can be concluded that the measured results in this study align well with the turbulence intensity values for Class C terrain specified in the Chinese, American, and Japanese standards, indicating good representativeness. The fitted relationship between turbulence intensity and gust factor is consistent with the commonly used Ishizaki and Choi empirical formulas. Before landfall, the mean turbulence integral scales at the 20 m height were 218 m and 100 m, respectively, and after landfall 198 and 177 m. No clear trend was observed in the turbulence integral scales with increasing mean wind speed.
3. The characteristics of the measured spectra under different mean wind speeds and turbulence integral scales are generally consistent before and after landfall. For the downwind wind speed spectrum, the Von Karman and Kaimal spectra show better agreement with the measured results compared to the Davenport spectrum. For the crosswind wind speed spectrum, the Von Karman spectrum aligns better with the measured results compared to the Kaimal spectra. Overall, the Von Karman spectrum better matches the measured near-surface turbulent wind speed spectrum characteristics.
4. There are still certain limitations in this wind field observation, including tower interference effects, having only one test data point, and the fact that the testing instrument can only observe two-dimensional wind fields.
5. For the changes in mean and turbulence wind field characteristics before and after the typhoon's landfall, a better explanation may be obtained by testing and analyzing the internal boundary layer (IBL) and atmospheric stability near the measurement point. However, this actual measurement has not yet considered it and developed a targeted testing plan, which is also research work that can be further carried out in the future.

Author Contributions: Conceptualization, X.L. (Xu Lei) and M.N.; methodology, X.L. (Xu Lei); software, X.L. (Xu Lei), X.L. (Xiaoyu Luo) and W.X.; validation, X.L. (Xu Lei) and L.S.; formal analysis, X.L. (Xu Lei) and L.S.; investigation, X.L. (Xu Lei); resources, M.N., X.L. (Xiaoyu Luo) and W.X.; data curation, X.L. (Xu Lei), X.L. (Xiaoyu Luo) and W.X.; writing—original draft preparation, X.L. (Xu Lei); writing—review and editing, X.L. (Xu Lei) and L.S.; visualization, X.L. (Xu Lei), Y.X. and L.S.; supervision, M.N. and X.L. (Xu Lei); project administration, X.L. (Xiaoyu Luo); funding acquisition, X.L. (Xu Lei), L.S. and Q.Y. All authors have read and agreed to the published version of the manuscript.

Funding: The work described in this article was supported by the National Natural Science Foundation of China (No. 52578551), Hunan Provincial Natural Science Foundation of China (No. 2022JJ40524, 2024JJ5049), Key research project of the Education Department of Hunan Province (No. 25A0631), Hunan Youth Talent Science and Technology Innovation Project (No. 2023RC3192), and Hunan Provincial Key Laboratory for Big Data Smart Application of Natural Disaster Risks Survey of Highway Engineering (No. BNH2024KFB010).

Institutional Review Board Statement: Not applicable.

Informed Consent Statement: Not applicable.

Data Availability Statement: The original contributions presented in this study are included in the article. Further inquiries can be directed to the corresponding authors.

Acknowledgments: This article also wishes to express gratitude to other colleagues from Guangdong Grid Co., Ltd. for their assistance and support during the on-site testing process.

Conflicts of Interest: The authors declare no conflicts of interest.

References

1. Lau, Y.; Yip, T.; Dulebenets, M.; Tang, Y.; Kawasaki, T. A review of historical changes of tropical and extra-tropical cyclones: A comparative analysis of the United States, Europe, and Asia. *Int. J. Environ. Res. Public Health* **2022**, *19*, 4499. [CrossRef]
2. Pang, J.; Lin, Z.; Ge, Y. Field measurements of strong wind characteristics near ground in Pudong district. *Exp. Meas. Fluid Mech.* **2002**, *16*, 32–39. [CrossRef]
3. Shi, W.; Li, Z.; Zhang, C. Field measurements of strong wind characteristics near ground in Wenzhou district. *J. Build. Struct.* **2010**, *31*, 34–40. [CrossRef]
4. Hu, S.; Song, L.; Li, Q. Monitoring of typhoons in surface boundary layer and analysis of wind turbulence characteristics. *J. Build. Struct.* **2011**, *32*, 1–8. [CrossRef]
5. Hu, S.; Li, Q.; Dai, Y.; Li, Z. Field measurement study on near ground wind characteristics and wind pressure of instrumented low rise building during typhoons. *J. Build. Struct.* **2013**, *34*, 30–38. [CrossRef]
6. Li, Q.; Dai, Y.; Li, Z.; Hu, S. Surface layer wind field characteristics during a severe typhoon 'Hagupit' landfalling. *J. Build. Struct.* **2010**, *31*, 54–61. [CrossRef]
7. Xiao, Y.; Li, L.; Song, L.; Qin, P. Study on wind characteristics of typhoon Hagupit based on offshore sea surface measurement. *Acta Aerodyn. Sin.* **2012**, *30*, 380–387+399. [CrossRef]
8. Li, L.; Xiao, Y.; Zhou, C.; Song, L. Modeling method for turbulent wind velocity spectrum in typhoon boundary layer based on conditions of design reference. *J. Vib. Shock* **2015**, *34*, 11–16. [CrossRef]
9. Xu, Z.; Wang, J.; Rao, H.; Dai, G. A study on near-ground turbulence power spectrum and its fitted parameters at Quanzhou Bay under the influence of typhoon "Bailu". *J. Vib. Shock* **2021**, *40*, 253–260. [CrossRef]
10. Wang, X.; Huang, P.; Gu, M.; Dai, Y. Field measurement of turbulence characteristics near ground during typhoon 'Meari'. *China Civ. Eng. J.* **2013**, *46*, 28–36. [CrossRef]
11. Wang, X.; Huang, P.; Gu, M. Field measurement on wind characteristics near ground during typhoon 'Muifa'. *China Civ. Eng. J.* **2013**, *46*, 54–61. [CrossRef]
12. Wang, X.; Huang, C.; Huang, P.; Zhou, H. Field measurements for characteristics of near ground turbulent wind during typhoon 'HAIKUI' blowing. *J. Vib. Shock* **2017**, *36*, 199–205+241. [CrossRef]
13. Li, B.; Zhang, X.; Yang, Q.; Yang, J. Research on turbulent wind characteristics near ground of typhoon 'Soulik' by field measurement. *J. Build. Struct.* **2015**, *36*, 99–104. [CrossRef]
14. He, H.; Lei, X.; Nie, M.; Xie, W.; Luo, X.; Su, C. Field Measurement Research of Near Ground Wind Field Characteristics in Landing Center during Typhoon 'Haima'. *J. Build. Struct.* **2018**, *39*, 29–36. [CrossRef]
15. Sun, F.; Xu, X.; Shi, W.; Zhu, Y.; Chen, L.; Li, Z.; Zhao, Z.; Jiang, S. Field measurements of typhoon characteristics near ground in Wenzhou coastal flat terrain. *Eng. Mech.* **2018**, *35*, 73–80+96. [CrossRef]
16. Shao, S.; Zhang, H.; Pan, F.; Yang, F.; Wang, F. Study on field measurements of strong wind characteristics near the typhoon "Mekkhala" landing place and design wind loads of transmission lines. *Proc. CSEE* **2021**, *41*, 4698–4710. [CrossRef]
17. Chen, F.; Weng, L.; Xiao, Y.; Li, Q. Field measurement of typhoon wind characteristics in offshore mountainous areas. *Eng. Mech.* **2021**, *38*, 33–41. [CrossRef]
18. Li, D.; Zhang, H.; Han, J. A study on near-earth wind profile characteristics of typhoon "Soulik" in southeast coastal area. *J. Vib. Shock* **2021**, *40*, 118–123+191. [CrossRef]

19. Huang, H.; Chen, W.; Zhi, S.; Wang, B. Analysis on severe wind characteristics during typhoon Rammasun landing process based on observation at observation tower. *Meteorol. Mon.* **2021**, *47*, 143–156. [CrossRef]
20. Zhang, J.; Wen, Z.; Lei, Y. Coastal near ground actually measured wind field characteristics in typhoon "Soudelor" moving process. *J. Vib. Shock* **2024**, *43*, 272–278+296. [CrossRef]
21. Cai, K.; Huang, M.; Wang, Y.; Ni, Y.; Chan, P.; Yang, H.; Wang, L. Research on statistical parameters of turbulent wind fields based on stationary and nonstationary models. *J. Southeast Univ. (Nat. Sci. Ed.)* **2025**, *55*, 1291–1300. [CrossRef]
22. Zeng, Y.; Wang, W.; Hu, J. Evolution Characteristics Analysis of Typhoon Mangkhut (1822). *J. Chengdu Univ. Inf. Sci. Technol.* **2021**, *36*, 86–94. [CrossRef]
23. Zhao, L.; Yang, X.; Fang, G.; Cui, W.; Song, L.; Ge, Y. Observation-based study for the evolution of vertical wind profiles in the boundary layer during super typhoon Mangkhut. *Acta Aerodyn. Sin.* **2019**, *37*, 43–54. [CrossRef]
24. He, Y.; Fu, J.; Li, Q.; Chen, P.; Chen, W. Field measurement of the global structure and wind field of typhoons in South China. *J. Aerodyn.* **2021**, *39*, 129–146. [CrossRef]
25. Xie, Z.; Duan, J.; Liu, M.; Zhang, L. Field measurement of near-ground wind characteristics of supper typhoon Mangkhut. *J. Tongji Univ. (Nat. Sci.)* **2021**, *49*, 652–660. [CrossRef]
26. Duan, J.; Zhang, L.; Xie, Z.; Liu, M. Nonatationary wind characteristics of typhoon Mangkhut. *J. Vib. Shock* **2022**, *41*, 18–26. [CrossRef]
27. Wang, X.; Liu, W.; Ye, Z.; Liu, L.; Mao, X. Field measurement of wind characteristics at long-span bridge site in coastal area during typhoon Mangkhut. *Bridge Constr.* **2021**, *51*, 29–36. [CrossRef]
28. Cui, Y.; Mao, X.; Sun, D.; Wang, X.; Li, Y. Study on the strong wind characteristics at the site of a cross sea bridge under the action of typhoon mangkhut. *Highway* **2022**, *67*, 116–122. [CrossRef]
29. Fang, P.; Zhao, B.; Zhang, S.; Zeng, Z.; Lin, W. An observation of the behavior of nearshore drag coefficient with moderate to strong wind speed. *J. Trop. Meteorol.* **2015**, *31*, 713–720. [CrossRef]
30. Liang, T.; Yu, X. A numerical study on thermal internal boundary layer over a coastal city. *Chin. J. Theor. Appl. Mech.* **2016**, *48*, 473–481. [CrossRef]
31. Li, T.; Qu, H.; Zhu, R.; Li, Y.; Tang, S. Near-surface wind-field characteristics of typhoon Morakot (2009) under different atmospheric stability conditions. *J. Aerodyn.* **2021**, *39*, 117–128. [CrossRef]
32. *GB50009-2012*; Load Code for the Design of Building Structures. China Architecture & Building Press: Beijing, China, 2012.
33. *ASCE/SEI 7-10*; Minimum Design Loads for Buildings and Other Structures. American Society of Civil Engineers: New York, NY, USA, 2010.
34. *AIJ-RLB-2004*; AIJ 2004 Recommendations for Loads on Buildings. Architectural Institute of Japan: Tokyo, Japan, 2004.
35. Ishizaki, H. Wind profiles, turbulence intensities and gustfactors for design in typhoon-prone regions. *J. Wind Eng. Ind. Aerodyn.* **1983**, *131*, 55–66. [CrossRef]
36. Choi, E.C.C. *Wind Loading in Hong Kong: Commentary on the Code of Practice on Wind Effects Hong Kong*; Hong Kong Institution of Engineers: Hong Kong, China, 1983.
37. Xiao, Y.; Sun, J.; Li, Q. Turbulence integral scale and fluctuation wind speed spectrum of typhoon: An analysis based on field measurements. *J. Nat. Disasters* **2006**, *15*, 45–53. [CrossRef]